ChemComm

COMMUNICATION

View Article Online
View Journal | View Issue

Cite this: *Chem. Commun.*, 2023, 59, 4927

Received 11th February 2023,
Accepted 16th March 2023

DOI: 10.1039/d3cc00629h

rsc.li/chemcomm

Surface modification enhances the bulk proton conductivity of Prussian blue†

Akira Takahashi, *[a] Yasuhito Matsubayashi, [b] Atsushi Sakurai,[a] Yutaka Sugiyama,[a] Keiko Noda[a] and Tohru Kawamoto [a]

Surface-modified Prussian blue shows 10^2 times higher bulk proton conductivity (0.018 S cm^{-1}) than that of unmodified Prussian blue. This enhancement is attributed to the monolayer adsorption of $Na_4[Fe(CN)_6]$ on the nanoparticle surface, which reduces the surface resistance. Surface modification is an effective strategy for improving bulk proton conductivity.

Highly proton-conductive materials are essential for building a sustainable society,[1] as they play a key role in various fuel cell systems.[2] Fuel cells are electrochemical energy converters[3] that produce limited pollution and have high energy conversion efficiency. In these systems, the proton conductor acts as the electrolyte, positioned between the anode and cathode.[4] Different types of proton conductor are used depending on the operating temperature of the fuel cell. For high temperatures (>600 °C), inorganic materials such as metal oxides are typically used. At low temperatures (<100 °C), aqueous solutions of alkaline hydroxides and perfluorosulfonic acids, such as Nafion, are employed. Although Nafion and other perfluorosulfonic acids exhibit proton conductivity of approximately 0.01–0.1 S cm^{-1} at room temperature,[5,6] they carry the potential risk of increasing the presence of per- and polyfluoroalkyl substances (PFAS),[7] which are bioaccumulative and cancer-inducing chemicals. Therefore, it is crucial to develop fluorine-free and low-cost proton conductors for use in fuel cells.

Metal organic frameworks (MOFs) have the potential to be used as proton conductors in the low temperature region owing to their ability to tune proton conductivity through the selection of metal and connecting ligands.[8] There several ways for improving proton conductivity of MOF, including modification of space and surface of pore,[9] defect,[10] and particle size.[11] Prussian blue (PB), a type of MOF, features a porous crystal structure composed of divalent and trivalent iron cations bridged by cyanide anions.[12] PB, which was discovered in the early 18th century, is traditionally used as a low-cost blue pigment.[13] PB and its analogues exhibit proton conductivity *via* the proton network formed by adsorbed water molecules within their porous crystal structure.[14,15] In addition, MOF with cyanide ligand, were developed for application using these proton conductivity.[16–19]

Efforts to enhance the proton conductivity of PB have been made by creating composites of PB analogues.[20–22] A study by Ono *et al.* showed that a grain-boundary-free PB nanofilm with a self-assembled monolayer exhibits high proton conductivity (approximately 0.1 S cm^{-1}).[23] However, proton conductors with bulk structures are more suitable for use in fuel cells than thin films. If PB can demonstrate such high proton conductivity in a bulk form, it can serve as a low-cost, fluorine-free electrolyte for fuel cells. Therefore, to achieve PB proton conductors with adequate proton conductivity in bulk form, three-dimensional (3D) aggregations of particles should be considered. Surface modification of nanoparticles has the potential to enhance bulk proton conductivity by improving the proton conductivity between nanoparticles of MOFs. Previous research has shown that surface modification with $Na_4[Fe(CN)_6]$ results in water-dispersible PB nanoparticles.[24] However, the effect of this surface modification on proton conductivity is yet to be evaluated.

In this study, we aimed to determine the quantitative effects of surface modification with $Na_4[Fe(CN)_6]$ on the proton conductivity of PB. Both non-dispersible and surface-modified dispersible PB nanoparticles were prepared, and their conductivity was compared to that of Nafion. Details of the preparation process can be found in Section S1 of the ESI.† PB nanoparticles were synthesised by mixing $Fe(NO_3)_{3aq}$ and $Na_4[Fe(CN)_6]_{aq}$ solutions. The PB nanoparticles without surface modification are referred to as PB-core. For surface modification, an additional amount of $Na_4[Fe(CN)_6]$ solution was mixed with the synthesised PB nanoparticles (Fig. 1(a)). The degree of surface modification is expressed as the atomic ratio of

[a] *Nanomaterials Research Institute, National Institute of Advanced Industrial Science and Technology (AIST), 1-1-1 Higashi, Tsukuba 305-8565, Japan. E-mail: akira-takahashi@aist.go.jp*
[b] *Device Technology Research Institute, National Institute of Advanced Industrial Science and Technology (AIST), 1-1-1 Higashi, Tsukuba 305-8565, Japan*

† Electronic supplementary information (ESI) available: Experimental section, Fig. S1–S5, Tables S1–S3. See DOI: https://doi.org/10.1039/d3cc00629h

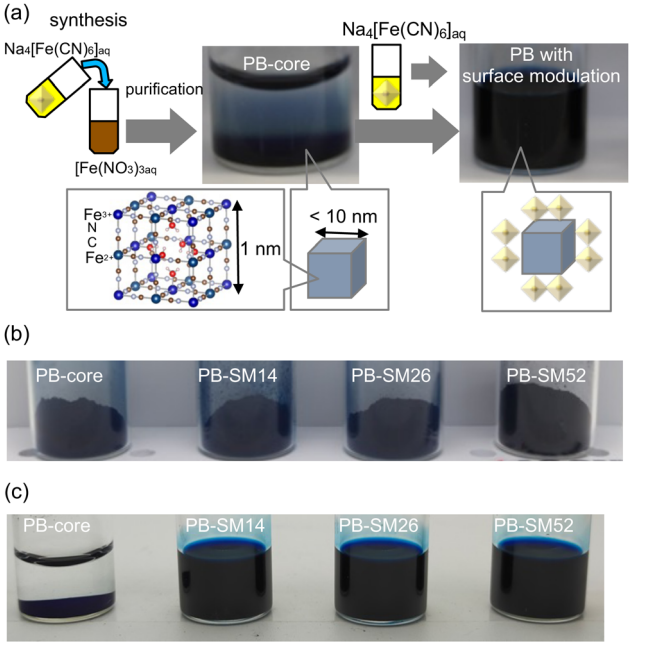

Fig. 1 (a) Synthesis procedure, (b) photographs of PB powders, and (c) photographs of PB powders in water.

additional $Na_4[Fe(CN)_6]$ to Fe^{3+} ($[Fe(CN)_6]/Fe^{3+}$, at%). Three groups of surface-modified PB nanoparticles were synthesised: PB-SM14 (14 at%), PB-SM26 (26 at%), and PB-SM52 (52 at%). After purification and drying, deep-blue PB powders were obtained (Fig. 1(b)). The FE-SEM image showed primary particle size of PBs, which were smaller than 10 nm (Section S3 of the ESI†). The PB-core nanoparticles precipitated in water, whereas the surface-modified PB nanoparticles were dispersible in water, similar to dispersible PB (Fig. 1(c)). The zeta potentials in water of PBs were as follows, PB-core: −23 mV, PB-SM14: −46 mV, PB-SM26: −45 mV, PB-52: −45 mV. The PB-core showed higher absolute value of zeta potentials than surface-modified PBs, resulting higher aggregated particle size of that in water (Fig. S2, ESI†).

The chemical composition of the samples was evaluated by microwave plasma atomic emission spectrometers and carbon, hydrogen, nitrogen analysis (Table 1). The PB-core sample had a similar composition to that of non-dispersible PB with a $[Fe(CN)_6]/Fe^{3+}$ ratio of 76 at%, indicating that the crystal structure contained 24% $[Fe(CN)_6]$ defects.

The surface-modified PBs had a higher $[Fe(CN)_6]/Fe^{3+}$ ratio than the PB-core sample because of the additional $Na_4[Fe(CN)_6]$ in the synthesis. Powder X-ray diffraction (PXRD) analysis showed that all the PB samples had a cubic crystal structure (space group: $Fm\bar{3}m$) with lattice constants of 1.017–1.026 nm, which is similar to the reported value.[12]

The crystallite size, as estimated from the PXRD patterns using Scherrer's equation, increased upon surface modification. The increase in crystallite size between the PB-core and PB-SM26 nanoparticles was 1.1 nm. This is close to the lattice constants of the PB unit cell, and suggests that the nanoparticles grew by half the length of the unit cell in each direction upon modification. This result is quantitively reasonable if we assume that a monolayer of $Na_4[Fe((CN)_6)]$ molecules covers the PB nanoparticles, as the half-unit-cell size corresponds to the length of the Fe^{2+}–CN–Fe^{3+} bond in $Na_4[Fe((CN)_6)$ (Fig. 1(a)). However Fe^{2+} at surface are covered by CN^- because the Fe^{2+} is a part of $[Fe(CN)_6]$, Fe^{3+} at surface can adsorb $Na_4[Fe((CN)_6)]$ with connecting CN^- of additional $[Fe(CN)_6]$. Thus, the additional $Na_4[Fe(CN)_6)]$ molecules likely adsorb at the Fe^{3+} sites on the nanoparticle surface.

The PB-core, PB-SM14, and PB-SM26 samples produced similar PXRD patterns and Fourier-transform infrared (FTIR) spectra (Fig. 2(a) and (b)). In contrast, those of the PB-SM52 sample also contained peaks of $Na_4[Fe(CN)_6]\cdot 10H_2O$ (indicated by red triangles in the figures), indicating that an excessive amount of $Na_4[Fe(CN)_6]$ was added during surface modification. The ideal amount of $Na_4[Fe\ (CN)_6]$ for surface modification (SM_{cal}) was estimated by counting the number of adsorption sites (Fig. 2(c), the crystal structure drawn with VESTA[25]). The $[Fe(CN)_6]^{4-}$ anions were assumed to adsorb at the Fe^{3+} sites on the PB surface, with a site density of 1.992 site nm^{-2} $[(1/4 \times 4 + 1)/(1.017^2) = 1.992]$. Assuming a PB crystallite size of 7.4 nm and crystal density of 1.78 g cm^{-3},[12] SM_{cal} was calculated as 23 at% $[Fe(CN)_6]/Fe^{3+}$. The calculation details are presented in Section S3 of the ESI.† Although this is only a rough approximation, the estimated SM_{cal} value was considered reasonable because it fell between the conditions used for producing the PB-SM14 and PB-SM26 samples, for which no $Na_4[Fe(CN)_6]\cdot 10H_2O$ was observed, indicating that all the additional $Na_4[Fe(CN)_6]$ was used for surface modification. The experimental results and estimated SM_{cal} value were used to illustrate the effect of additional $Na_4[Fe(CN)_6]\cdot 10H_2O$ in each PB sample, as shown in Fig. 2(d).

To form bulk samples from the PB powders with different surface modifications, the PB powders were formed into bulk samples by a moulding method (details can be found in Section S6 of the ESI†). This method is easier than the pellet method, in which bulk conductivity is evaluated after compacting the powder into a pellet, as the pellets require sufficient hardness for evaluation. We confirmed that the mould method provides

Table 1 Sample list with magnitude of surface modification, chemical composition, lattice constant, and crystallite size

	Surface modulation at% $[Fe(CN)_6]/Fe^{3+}$	Chemical composition	Lattice constant (nm)	Crystallite size (nm)
PB-core	—	$Fe[Fe(CN)_6]_{0.76}\ 5.4H_2O$	1.017	7.4
PB-SM14	14	$Na_{0.71}Fe[Fe(CN)_6]_{0.95}\ 5.3H_2O$	1.021	7.6
PB-SM26	26	$Na_{1.10}Fe[Fe(CN)_6]_{0.97}\ 5.0H_2O$	1.023	8.5
PB-SM52	52	$Na_{2.41}Fe[Fe(CN)_6]_{1.45}\ 7.4H_2O$	1.026	8.4

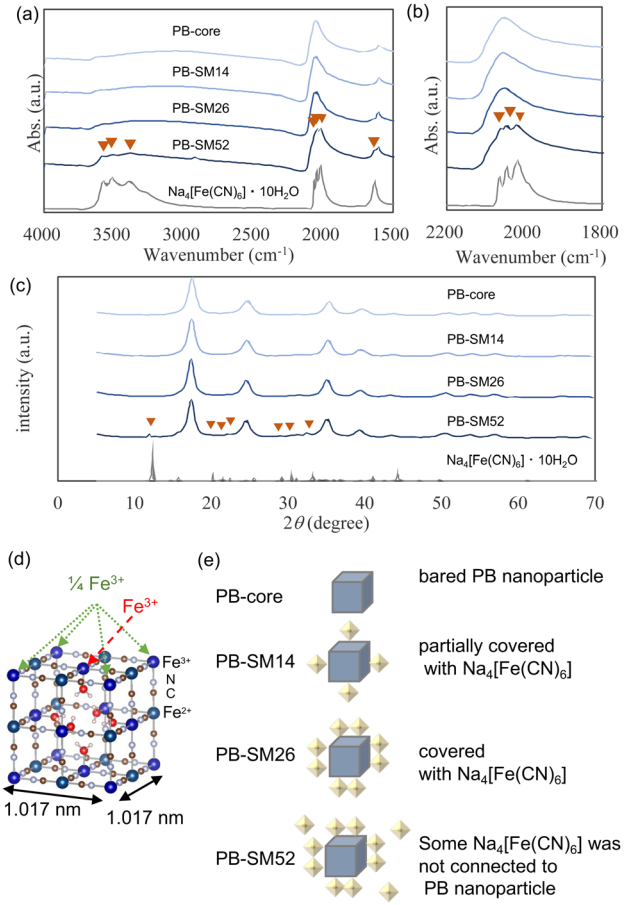

Fig. 2 (a) and (b) FTIR spectra and (c) PXRD of PBs and $Na_4[Fe(CN)_6]$ $10H_2O$. same peak of $Na_4[Fe(CN)_6]$ $10H_2O$ in PB were signed with triangles. (d) counting Fe^{3+} site on the surface of PB with unit cell. (e) speculated surface image of PBs.

the same ion conductivity results as the pellet method for ion-conducting materials (Section S6-3 of the ESI†).

The bulk proton conductivities were evaluated by measuring the impedance under N_2 gas flow at 95% relative humidity and room temperature (around 20 °C). The real and imaginary parts of impedance (Z) for each PB sample are shown in the Cole–Cole plots in Fig. 3(a). Semi-circular regions were observed for all PBs, which arise due to proton conduction.

The proton conductivities were estimated by fitting the circular arc intercepts on the Z' axis of the graph. The results in Fig. 3(b) show that the bulk proton conductivity increased upon surface modification and reached saturation at around PB-SM26. The bulk conductivity of PB-SM26 (0.018 S cm^{-1}) was 10^2 times higher than that of the PB-core (1.7×10^{-4}). The lower proton conductivity of PB-SM14 compared to those of PB-SM26 and PB-SM52 indicates that the surface of PB-SM14 is partially occupied by $Na_4[Fe(CN)_6]$ (Fig. 2(d)). The bulk conductivity of PB-SM52 was as much as PB-SM26, however PB-SM52 contained higher amount of $Na_4[Fe(CN)_6]$. It was because that some amount of $Na_4[Fe(CN)_6]$ contributed to the modification but remained as crystal, which was observed with PXRD and FTIR (Fig. 2(a–c)). This enhancement with surface

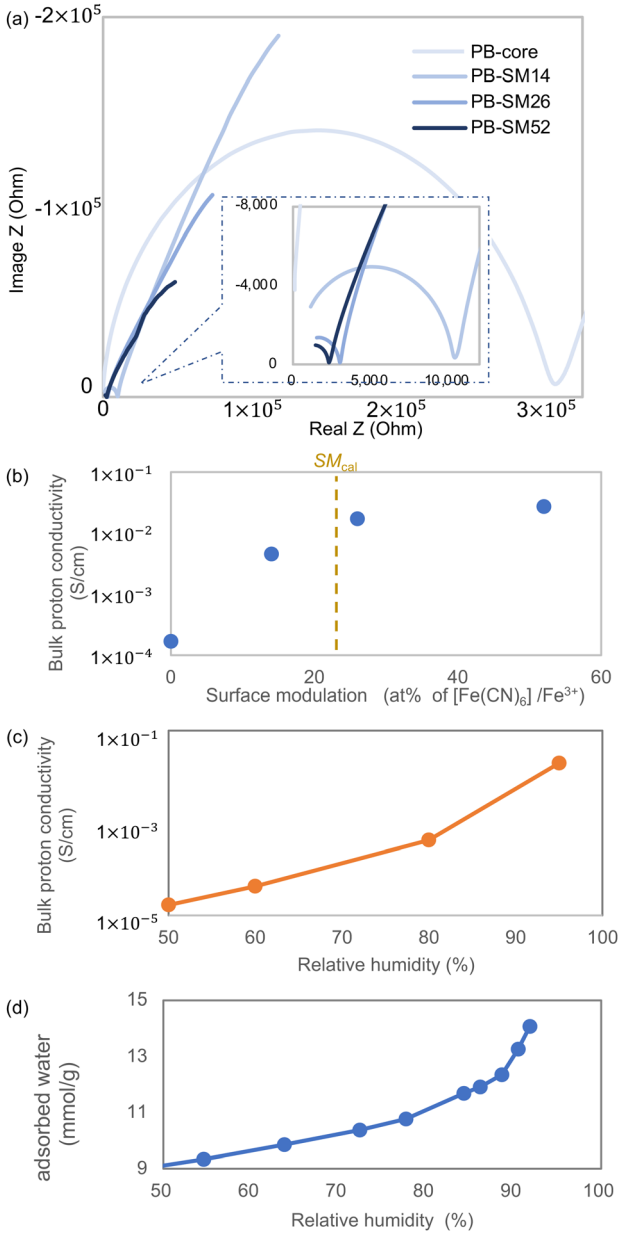

Fig. 3 (a) Cole–Cole plot of PBs at 95% relative humidity and room temperature. (b) Relationship between surface modification and bulk proton conductivity. (c) Effect of humidity on bulk proton conductivity of PB-SM26.

modification was also observed in other PB analogues (Fig. S6-4 in the ESI†).

To investigate the response to humidity, the bulk proton conductivity of PB-SM26 was evaluated at various relative humidities. The results showed that the conductivity increased with humidity, similar to previous reports of proton conductors, as shown in Fig. 3(c). Proton conductivity in PB and its analogues reportedly occurs *via* the Grotthus mechanism.[14,26] In this mechanism, protons are transported by a hydrogen network of water molecules in the crystal structure. The number of adsorbed water molecules in PB increases with humidity,

leading to an increase in the number of hydrogen bonds in the network and thus the proton conductivity.

Previously, the logarithm of the bulk proton conductivity of PB analogues was found to be linearly proportional to humidity. However, the proton conductivity of PB-SM26 displayed a sudden increase between 80% and 95% relative humidity, resulting in a high proton conductivity comparable to that of Nafion. In previous reports, grain-boundary-free PB nanofilms exhibited nonlinear curves,[23] suggesting that the nonlinearity observed for the PB nanoparticles might be attributed to surface effects.

Although PB analogues and other MOFs conduct protons *via* their porous crystal structures, the bulk proton conductivity of PB was enhanced by surface modification with $Na_4[Fe(CN)_6]$. We speculate that surface modification with $Na_4[Fe(CN)_6]$ makes the surface hydrophilic, thereby facilitating the adsorption of water compared to that for non-dispersible PB. The water adsorption isotherm at 25 °C shows a sudden increase as much as proton conductivity at around 90 RH% (Fig. 3(d)). The results would suggest that the sudden increase of water adsorption was due to capturing water at the hydrophilic surface modified with $Na_4[Fe(CN)_6]$. Consequently, the modified nanoparticles adsorb a greater amount of water, which reduces their surface resistance. This in turn may enhance proton conductivity not only at the interface between the electrode and nanoparticles, but also within the crystal structure and between nanoparticles, resulting in enhanced bulk conductivity. Because this enhancement is based on surface modification of particles, it is considered to be more effective when the particle size is smaller.

In conclusion, this study demonstrated the surface modification of PB nanoparticles with varying intensities of $Na_4[Fe(CN)_6]$. The observed increase in crystallite size and ideal amount of $Na_4[Fe(CN)_6]$ support the proposed mechanism of surface modification. The results showed that surface modification improved the proton conductivity, with PB-SM26 exhibiting the highest improvement of 10^2 times compared to that of unmodified PB. This improvement is attributed to the reduced surface resistance between nanoparticles caused by the adsorption of a $Na_4[Fe(CN)_6]$ monolayer. The saturation of the $Na_4[Fe(CN)_6]$ monolayer for PB-SM26 is believed to have contributed to its exceptional proton conductivity. This study provides a promising approach for enhancing the bulk proton conductivity of PB and its analogues. It seems to be effective for other proton conductors which have restriction of high surface resistance.

A. Takahashi, Y. Matsubayashi, A. Sakurai, K. Noda, and Y. Sugiyama were contributed to measurements of bulk conductivity, characterization of samples. A. Takahashi and T. Kawamoto contributed to design of experiments.

This work was supported by JSPS KAKENHI Grant Number JP19K15594. We appreciate to the support of measuring zeta potential from Dr Yoshie Ishihara.

Conflicts of interest

There are no conflicts to declare.

References

1 K.-D. Kreuer, *Chem. Mater.*, 1996, **8**, 610–641.
2 G. Centi and S. Perathoner, *Catal. Today*, 2009, **148**, 191–205.
3 O. Z. Sharaf and M. F. Orhan, *Renewable Sustainable Energy Rev.*, 2014, **32**, 810–853.
4 B. C. H. Steele and A. Heinzel, *Nature*, 2001, **414**(6861), 345–352.
5 B. Dong, L. Gwee, D. Salas-De La Cruz, K. I. Winey and Y. A. Elabd, *Nano Lett.*, 2010, **10**, 3785–3790.
6 L. Liu, W. Chen and Y. Li, *J. Membr. Sci.*, 2016, **504**, 1–9.
7 M. Feng, R. Qu, Z. Wei, L. Wang, P. Sun and Z. Wang, *Sci. Rep.*, 2015, **5**(51), 1–8.
8 M. Yoon, K. Suh, S. Natarajan and K. Kim, *Angew. Chem., Int. Ed.*, 2013, **52**, 2688–2700.
9 M. K. Sarango-Ramírez, J. Park, J. Kim, Y. Yoshida, D.-W. Lim, H. Kitagawa, M. K. Sarango-Ramírez, Y. Yoshida, H. Kitagawa, J. Park, J. Kim and D. Lim, *Angew. Chem., Int. Ed.*, 2021, **60**, 20173–20177.
10 J. M. Taylor, S. Dekura, R. Ikeda and H. Kitagawa, *Chem. Mater.*, 2015, **27**, 2286–2289.
11 D. A. Levenson, J. Zhang, B. S. Gelfand, S. P. Kammampata, V. Thangadurai and G. K. H. Shimizu, *Dalton Trans.*, 2020, **49**, 4022–4029.
12 H. J. Buser, D. Schwarzenbach, W. Petter and A. Ludi, *Inorg. Chem.*, 1977, **16**, 2704–2710.
13 A. Kraft, *Bull. Hist. Chem.*, 2008, **33**, 61–67.
14 S. I. Ohkoshi, K. Nakagawa, K. Tomono, K. Imoto, Y. Tsunobuchi, H. Tokoro, K. Tomon, K. Imoto, Y. Tsunobuchi, H. Tokoro, K. Tomono, K. Imoto, Y. Tsunobuchi and H. Tokoro, *J. Am. Chem. Soc.*, 2010, **132**, 6620–6621.
15 J. Vega-Moreno, A. A. Lemus-Santana, E. Reguera, A. Andrio and V. Compañ, *Electrochim. Acta*, 2020, **360**, 136959.
16 M. Reczyński, B. Nowicka, C. Näther, M. Kozieł, K. Nakabayashi, S. I. Ohkoshi and B. Sieklucka, *Inorg. Chem.*, 2018, **57**, 13415–13422.
17 J. Wang, J. J. Zakrzewski, M. Heczko, M. Zychowicz, K. Nakagawa, K. Nakabayashi, B. Sieklucka, S. Chorazy and S. I. Ohkoshi, *J. Am. Chem. Soc.*, 2020, **142**, 3970–3979.
18 Y. Zhou, H. Xiang, J. Y. Zhu, L. Shi, W. J. You, X. Q. Wei, Z. Tian and D. Shao, *Polyhedron*, 2022, **228**, 116181.
19 Y. Hu, Z. Guo, Y. Chen, C. Zhou, Y. C. Li and S. Ren, *Nat. Commun.*, 2022, **13**, 7056.
20 Q. Qiao, H. J. Wang, C. P. Li, X. Z. Wang and X. M. Ren, *Inorg. Chem. Front.*, 2021, **8**, 2305–2314.
21 Y. Yin, M. Li, X. Liu, N. Xie, C. Zheng, G. Liu, S. Yin, X. Li, Y. Pei, J. Zhang, Y. Qin and M. D. Guiver, *J. Power Sources*, 2022, **537**, 231542.
22 X. Liu, J. Zhang, C. Zheng, J. Xue, T. Huang, Y. Yin, Y. Qin, K. Jiao, Q. Du and M. D. Guiver, *Energy Environ. Sci.*, 2020, **13**, 297–309.
23 K. Ono, M. Ishizaki, K. Kanaizuka, T. Togashi, T. Yamada, H. Kitagawa and M. Kurihara, *Angew. Chem.*, 2017, **129**, 5623–5627.
24 A. Gotoh, H. Uchida, M. Ishizaki, T. Satoh, S. Kaga, S. Okamoto, M. Ohta, M. Sakamoto, T. Kawamoto, H. Tanaka, M. Tokumoto, S. Hara, H. Shiozaki, M. Yamada, M. Miyake and M. Kurihara, *Nanotechnology*, 2007, **18**, 345609.
25 K. Momma and F. Izumi, *J. Appl. Crystallogr.*, 2011, **44**, 1272–1276.
26 N. Agmon, *Chem. Phys. Lett.*, 1995, **244**, 456–462.

